Helical structures in layered magnetic superconductors due to indirect exchange interactions mediated by interlayer tunneling

A. E. Koshelev

Phys. Rev. B **100**, 224503 — Published 5 December 2019

DOI: 10.1103/PhysRevB.100.224503

Helical structures in layered magnetic superconductors due to indirect exchange interactions mediated by interlayer tunneling

A. E. Koshelev
Materials Science Division, Argonne National Laboratory, Lemont, Illinois 60439
(Dated: November 18, 2019)

Motivated by the recent discovery of helical magnetic structure in $RbEuFe_4As_4$, we investigate interlayer ordering of magnetic moments in materials composed of spatially-separated superconducting and ferromagnetically-aligned layers. We consider the interplay between the normal and superconducting indirect exchange interaction mediated by tunneling between the conducting layers. We elaborate a recipe to evaluate the normal interlayer interaction via two-dimensional density of states of an isolated layer and demonstrate that for bands with small fillings, such interaction is typically ferromagnetic and short-range. The nearest-layer interaction is proportional to the ratio of the interlayer hopping and in-plane band width squared. On the other hand, the superconducting contribution always gives antiferromagnetic interaction and may extend over several layers when the interlayer hopping energy exceeds the superconducting gap. The frustration caused by the interplay between the normal and superconducting parts may lead to spiral ground-state magnetic configuration. The four-fold in-plane anisotropy may lock the rotation angle between the moments in the neighboring layers to 90°, as it was observed in $RbEuFe_4As_4$.

I. INTRODUCTION

Europium-based iron pnictides have been introduced recently as a new platform to investigate the interplay between singlet superconductivity and magnetic order [1–10]. Superconducting and ferromagnetic phases are two common electronic ground states of conducting materials antagonistic to each other. Their mutual influence causes many interesting phenomena which have been thoroughly investigated for a half century [11–17].

Coexistence of uniform superconducting and ferromagnetic states is usually energetically unfavorable. The coupling between these subsystems at the microscopic level is due to the exchange interaction of conducting electrons with localized moments. In normal state, such local coupling generates indirect interaction between the moments mediated by the mobile electrons known as Ruderman-Kittel-Kasuya-Yosida (RKKY) interaction [18]. Additionally, the superconducting response to the magnetic field generated by the aligned moments leads to the macroscopic electromagnetic interaction between the superconducting and magnetic subsystems [19, 20]. The common nonuniform ground-state configuration depends on the relative strength of these two interaction channels as well as on the relative strength of superconductivity and magnetism.

The superconducting order strongly modifies the RKKY interaction at large distances. Anderson and Suhl [21] demonstrated that this modification may lead to "cryptoferromagnetic" state in which the ferromagnetic subsystem is split into a periodic array of small domains facilitating coexistence with superconductivity. The domain size is determined by the interplay between the short-range normal and long-range superconducting RKKY interactions. In isotropic materials, it is expected to be much smaller than the superconducting coherence length but much larger than the distance between the localized moments and the Fermi wavelength. A particular realization of such oscillatory magnetic state depends on the properties of the magnetic subsystem. In the case of weak magnetic anisotropy, the helical structure may be formed instead. A detailed theory of such structure has been elaborated in Ref. [22] for the case of the isotropic electronic spectrum. Similar nonuniform magnetic states have also been predicted for the case of purely electromagnetic coupling between the subsystems [23, 24]. Alternatively, a hard magnetic subsystem remaining uniform itself may make the superconducting system nonuniform via generation of spontaneous vortex lines [19, 20].

Several classes of superconducting materials with long-range magnetic order are known at present. In most materials, the magnetism is hosted by rare-earth elements which are sufficiently separated from the conducting electrons so that the exchange interaction is relatively weak and does not destroy superconductivity. Two first such groups of materials discovered in the 1970s are ternary molybdenum chalcogenides $RE\mathrm{Mo}_6X_8$ (RE=rare-earth element and X=S, Se) also known as Chevrel phases and ternary rhodium borides $RE\mathrm{Rh}_4\mathrm{B}_4$. The detailed description of their properties may be found in reviews [12, 17] and in the book [25]. While most of these materials have antiferromagnetic order in the superconducting state, two notable exceptions are $\mathrm{ErRh}_4\mathrm{B}_4$ with $T_c \approx 8.5$K[26] and $\mathrm{Ho}_{1.2}\mathrm{Mo}_6\mathrm{S}_8$ with $T_c \approx 1.2$K[27], where superconductivity competes with the long-range ferromagnetic order. The emerging ferromagnetism at sub-Kelvin temperatures leads to the reentrance of the normal state and formation of the intermediate oscillatory magnetic state in the narrow coexistence region, in qualitative agreement with theory [21, 22]. The similar reentrant behavior was also found in the rhodium stannide $RE\mathrm{Rh}_{1.1}\mathrm{Sn}_{3.6}$ [28].

Two decades later, during the 1990s, the rare-earth nickel borocarbides $RE\mathrm{Ni}_2\mathrm{B}_2\mathrm{C}$ have been added to the family of magnetic superconductors, see reviews [15, 16,

29, 30]. Distinctive features of these materials significantly expanded and enriched the field of coexistence of superconductivity and magnetic order. In contrast to the above cubic ternary compounds, these materials have layered structure: they are composed of conducting Ni layers and magnetic REC layers. In spite of such a structure, the electronic anisotropy is small. In compounds with RE=Tm, Er, Ho, and Dy, the superconductivity coexists with different kinds of magnetic order and every compound has some unique features. In most cases the magnetic moments are aligned within REC layers and alternate from layer to layer (A-type antiferromagnets). In all compounds except the Tm one the moments are oriented along the layers. In $HoNi_2B_2C$ the transition to such state occurs via the two intermediate incommensurate spiral configurations. Magnetic structure in $ErNi_2B_2C$ is characterized by additional in-plane modulation, which is likely induced by coupling to the superconducting subsystem. In addition, a weak ferromagnetic state emerges in this material below 2.3K at the second magnetic transition, and this state coexists with superconductivity at lower temperatures.

All discussed materials are conventional singlet superconductors. The triplet superconducting state, in which Cooper pairs are formed by electrons with the same spin, is less hostile to ferromagnetism than the singlet state. The likely candidates for the triplet state are uranium-based compounds UGe_2, URhGe, and UCoGe discovered in the 2000s, see reviews [31, 32]. The superconducting transitions in these compounds take place in sub-Kelvin temperature range, inside the ferromagnetic state. For such low transition temperatures, the superconductivity survives up to remarkably high magnetic field, 10-25 teslas, which is attributed to the triplet pairing.

Recent development in the field is related to discovery and characterization of magnetically-ordered iron pnictides, in particular, europium-based 122 compounds, see review [10]. As the borocarbides, these materials have layered structure: they are composed of the spatially separated magnetic Eu and conducting FeAs layers. The tunneling between the FeAs layers is rather strong so that the electronic anisotropy is also small. The parent non-superconducting material $EuFe_2As_2$ [1, 3, 33] develops the spin-density wave order in the FeAs layers at 189K and the A-type antiferromagnetic order in the Eu^{2+} layers at 19K with the magnetic moments oriented along the layers. It becomes superconducting under pressure with the maximum transition temperature reaching 30K at 2.6 GPa, so that the magnetic transition takes place in the superconducting state [34]. Several substitutions also give superconductors coexisting with Eu magnetic order: (i)K[2] and Na[35] on Eu site, (ii)Ir[36], Ru[37], and Co[38] on Fe site, and (iii)P on As site[4–6, 39–41]. The maximum superconducting transition temperature for different substitution series ranges from 22 to 35K exceeding the magnetic-transition temperature in Eu layers. Therefore the unique feature of these materials is that they exhibit Eu^{2+} magnetism at the temperature scale, comparable with the superconducting transition.

The most investigated substituted compound is $EuFe_2(As_{1-x}P_x)_2$. For optimal substitution, $x \approx 0.3$, it has the superconducting transition at 26K followed by the ferromagnetic transition at 19K. At lower temperatures, ferromagnetism coexists with superconductivity. In contrast to the parent compound, the Eu moments are oriented along the c axis [41]. This leads to the formation of the composite domain and vortex-antivortex structure visualized by the decorations [42] and magnetic-force microscopy [43]. This structure has been attributed to purely electromagnetic coupling between the magnetic moments and superconducting order parameter [44]. Alternatively, it also may be the realization of the "cryptoferromagnetic" state caused by the weak exchange interaction [21].

The most recent development in the field is synthesis of the stoichiometric compounds $A EuFe_4As_4$ with A=Rb [8, 9, 45–47] and Cs [7, 9] in which every second layer of Eu is completely substituted with Rb or Cs. These 1144 materials have the superconducting transition temperature of 36.5 K, higher than the doped 122 Eu compounds. On the other hand, the magnetic transition temperature is 15K, which is 4K lower than in $EuFe_2As_2$, most likely because of the weaker interaction between the magnetic layers. These materials are characterized by low superconducting anisotropy ~ 1.7 and highly-anisotropic easy-axis Eu magnetism [46, 48]. With increasing pressure the superconducting temperature is suppressed and the magnetic temperature is enhanced so that they cross at $\sim$ 7GPa and at higher pressures superconducting transition takes place in the magnetically-ordered state [49, 50]. Recent resonant X-ray scattering and neutron diffraction measurements revealed that the magnetic structure is helical: the Eu moments rotate 90° from layer to layer [51, 52], see the picture in Fig. 1.

Motivated by this unexpected finding, we investigate magnetic structure in a material composed of spatially separated ferromagnetically-aligned and superconducting layers. Due to the large separation, the interaction between different Eu layers in $A EuFe_4As_4$ most likely has the RKKY origin. As the Eu 4f orbitals are strongly localized, one can only consider interaction with the closest FeAs layers. An essential feature of the $A EuFe_4As_4$ structure is that the neighboring Eu layers have a direct coupling with different FeAs layers, see the picture in Fig. 1. Consequently, the magnetic interlayer interaction is mediated by tunneling between the conducting layers. As these materials are not very anisotropic, this mechanism is not particularly weak. In contrast, the Eu-122 compounds and borocarbides are composed of alternating magnetic and conducting layers. In this case, two adjacent magnetic layers couple with the same conducting layer yielding a finite interlayer interaction even without tunneling between the conducting layers.

One may think that a possible alternative to the RKKY mechanism may be the electromagnetic dipole interactions. We note, however, that the dipole interaction

between uniformly polarized layers is very small when separation between them exceeds the in-plane distance between the moments a. Indeed, the average magnetic field outside of a uniformly polarized layer is zero and the oscillating component decays away from the layer very fast, as $\exp(-2\pi z/a)$ [53]. For distances z much smaller than the London penetration depth, superconductivity has a very weak influence on this behavior. In the case of $A\mathrm{EuFe_4As_4}$, $a = 3.9\mathring{A}$ and the separation between the magnetic layers is $c = 13.3\mathring{A}$ [7]. This means that the exponential factor is estimated as $\exp(-2\pi c/a) \approx 4.6 \cdot 10^{-10}$, i.e., the dipole interaction is negligible even for neighboring layers.

We consider magnetic structure appearing as a result of the interplay between the normal and superconducting RKKY interactions mediated by tunneling between the conducting layers. To highlight essential physics, we mostly study a relatively simple single-band model with open Fermi surface. We relate the normal interlayer interaction with the two-dimensional density of states of an isolated layer. An important observation is that this interaction vanishes for quadratic in-plane spectrum corresponding to the energy-independent density of states. In the case of a shallow band when non-parabolicity is small, the normal-state interlayer interaction is ferromagnetic and short-range. Such behavior is very different from the oscillatory in-plane RKKY interaction, which has been investigated for the iron pnictides and selenides in Ref. [54]. The superconducting contribution always gives antiferromagnetic interlayer interaction that may extend over several layers when the interlayer hopping exceeds the superconducting gap. As a result of frustrating interlayer interactions caused by the interplay between the normal and superconducting parts, the ground-state magnetic configuration may be a helix. A similar physical mechanism of the helical magnetic structure in $\mathrm{RbEuFe_4As_4}$ has been proposed in the recent paper [55] based on the earlier results obtained for isotropic electronic spectrum [22]. We point, however, that the layered structure and open Fermi surface lead to qualitative modifications of both normal and superconducting RKKY interactions, which are in the focus of this paper. In general, the rotation angle between the moments in the neighboring layers continuously varies with the model parameters. The 90° helix observed in $\mathrm{RbEuFe_4As_4}$ is most likely related to the in-plane four-fold anisotropy which locks such structure within a finite range of parameters.

The paper is organized as follows: In Sec. II, we introduce the model. In Secs. III and IV, we consider the normal and superconducting interactions between magnetic layers mediated by the indirect exchange due to tunneling between the conducting layers. In Sec. V, we discuss generalization of these results to multiple-band materials. In Secs. VI and VII, we compute the energy of helical structure and the optimal modulation vector.

II. MODEL

We consider a material composed of superconducting and magnetic layers. The local moments inside the magnetic layers are assumed to be ordered ferromagnetically. The major focus of this paper is the interlayer magnetic order emerging due to the interplay between the normal and superconducting RKKY interactions. The system under consideration is described by the Hamiltonian

$$\hat{H} = \hat{H}_S + \hat{H}_M + \hat{H}_{MS}, \tag{1}$$

where the first term

$$\begin{aligned}\hat{H}_S = \sum_n \int d^2\boldsymbol{r} \Big[& \psi^\dagger_{n,\alpha}(\boldsymbol{r})\hat{\xi}_{2D}\psi_{n,\alpha}(\boldsymbol{r}) \\ & -t_\perp \left(\psi^\dagger_{n,\alpha}(\boldsymbol{r})\psi_{n+1,\alpha}(\boldsymbol{r}) + \psi^\dagger_{n+1,\alpha}(\boldsymbol{r})\psi_{n,\alpha}(\boldsymbol{r})\right) \\ & - \frac{g}{2}\psi^\dagger_{n,\alpha}(\boldsymbol{r})\psi^\dagger_{n,\beta}(\boldsymbol{r})\psi_{n,\beta}(\boldsymbol{r})\psi_{n,\alpha}(\boldsymbol{r})\Big]\end{aligned} \tag{2}$$

describes the superconducting subsystem. Here α, β are spin indices, $\hat{\xi}_{2D} = \xi_{2D}(\hat{\boldsymbol{p}}) = \varepsilon_{2D}(\hat{\boldsymbol{p}}) - \varepsilon_F$ is the single-layer spectrum, and $t_\perp$ is the interlayer hopping energy. For bands with low fillings, this spectrum can be approximated as quadratic, $\varepsilon_{2D}(\boldsymbol{p}) = p^2/2m$. The full three-dimensional electronic spectrum of this model is

$$\varepsilon(\boldsymbol{p}, q) = \varepsilon_{2D}(\boldsymbol{p}) + \varepsilon_z(q), \tag{3}$$

where for the assumed simplest interlayer tunneling $\varepsilon_z(q) = -2t_\perp \cos q$ with q being the reduced c-axis wave vector, $-\pi < q < \pi$. Such spectrum for $\varepsilon_F > 2t_\perp$ corresponds to open Fermi surface. The second term $\hat{H}_M$ in Eq. (1) describes the magnetic layers favoring ferromagnetic alignment of the moments inside them. Its particular form does not play a role in our consideration. In the case of $\mathrm{RbEuFe_4As_4}$, the thermodynamics of the magnetic transition is well described by the easy-plane quasi-two-dimensional Heisenberg model [48].

The interaction between the superconducting and magnetic subsystems is determined by the local exchange Hamiltonian

$$\hat{H}_{MS} = \sum_{n,m}\int d^2\boldsymbol{r}\sum_{\boldsymbol{R}} \psi^\dagger_{n,\alpha}(\boldsymbol{r})J_{nm}(\boldsymbol{r}-\boldsymbol{R})\boldsymbol{\sigma}_{\alpha\beta}\boldsymbol{S}_m(\boldsymbol{R})\psi_{n,\beta}(\boldsymbol{r}), \tag{4}$$

where $\boldsymbol{S}_m(\boldsymbol{R})$ are localized spins and $\boldsymbol{\sigma}_{\alpha\beta}$ is the Pauli-matrix vector. We can rewrite $\hat{H}_{MS}$ as

$$\hat{H}_{MS} = -\sum_n \int d^2\boldsymbol{r}\psi^\dagger_{n,\alpha}(\boldsymbol{r})\boldsymbol{h}_n(\boldsymbol{r})\boldsymbol{\sigma}_{\alpha\beta}\psi_{n,\beta}(\boldsymbol{r}),$$

where

$$\boldsymbol{h}_n(\boldsymbol{r}) = -\sum_m \sum_{\boldsymbol{R}} J_{nm}(\boldsymbol{r}-\boldsymbol{R})\boldsymbol{S}_m(\boldsymbol{R}) \tag{5}$$

is the effective exchange field acting on spins of conducting electrons[1]. The fermionic response to such a field in both normal and superconducting state is determined by the nonlocal spin susceptibility $\chi_n(\boldsymbol{r})$ and at fixed arrangements of the localized moments the corresponding energy contribution is

$$E_{MS} = -\frac{1}{2}\sum_{n,n'}\int d^2\boldsymbol{r}\int d^2\boldsymbol{r}'\chi_{n-n'}(\boldsymbol{r}-\boldsymbol{r}')\boldsymbol{h}_n(\boldsymbol{r})\boldsymbol{h}_{n'}(\boldsymbol{r}'). \tag{6}$$

In superconducting state, the assumed linear-response approximation is valid if the amplitude of the exchange field h is smaller than the superconducting gap Δ.

In this paper we focus on the case when the localized spins are ferromagnetically aligned inside the layers, i.e., $\boldsymbol{S}_m(\boldsymbol{R})$ is in-plane coordinate independent. In this case $\boldsymbol{h}_n(\boldsymbol{r})$ also becomes uniform, $\boldsymbol{h}_n(\boldsymbol{r}) \to \boldsymbol{h}_n = -\sum_m \mathcal{J}_{nm}\boldsymbol{S}_m$ with $\mathcal{J}_{nm} = \sum_{\boldsymbol{R}} J_{nm}(\boldsymbol{r}-\boldsymbol{R})$ being the total exchange interaction from all aligned spins in a single layer. In this case, Eq. (6) gives the following result for the energy per unit area per magnetic layer

$$\begin{aligned} F_{MS} &= -\frac{1}{2N_M}\sum_{n,n'}\mathcal{X}_{n-n'}\boldsymbol{h}_n\boldsymbol{h}_{n'} \\ &= -\frac{1}{2N_M}\sum_{m,m'}\mathcal{I}_{m-m'}\boldsymbol{S}_m\boldsymbol{S}_{m'} \end{aligned} \tag{7}$$

where N_M is the total number of magnetic layers,

$$\mathcal{X}_n = \int d\boldsymbol{r}\chi_n(\boldsymbol{r}) \tag{8}$$

is the nonlocal susceptibility integrated over the in-plane coordinate, and

$$\mathcal{I}_{m-m'} = \sum_{n,n'}\mathcal{X}_{n-n'}\mathcal{J}_{nm}\mathcal{J}_{n'm'} \tag{9}$$

are the effective interlayer interaction constants. Being mediated by the conduction electrons, these constants have an RKKY nature. For brevity, in the following consideration we refer to the quantity $\mathcal{X}_n$ in Eq. (8) as an interlayer susceptibility.

We consider the situation when (i)RKKY is the dominating mechanism and therefore Eqs. (7) and (9) determine the interlayer magnetic structure and (ii)different magnetic layers are not coupled with the same metallic layer, i.e., $\sum_n \mathcal{J}_{nm}\mathcal{J}_{nm'} = 0$ for $m \neq m'$ and the interlayer interactions only appear due to tunneling between the metallic layers yielding finite $\mathcal{X}_n$ for $n \neq 0$. The latter situation is realized in the magnetic 1144 iron arsenides. In the case of $RbEuFe_4As_4$, due to the strongly localized nature of the $4f$ states, one can only take into account the exchange interactions with closest metallic layers. Therefore, we may only consider interactions of a Eu layer with index m with the two neighboring FeAs layers with the indices $n = 2m-1$ and $2m$, see the picture in Fig. 1. Dropping the indices in these nearest-neighbor exchange constants $\mathcal{J}_{nm}$, we evaluate from Eq. (9)

$$\mathcal{I}_l \approx \mathcal{J}^2\sum_{\delta,\delta'=0,1}\mathcal{X}_{2l-\delta+\delta'} = \mathcal{J}^2\left(\mathcal{X}_{2l-1}+2\mathcal{X}_{2l}+\mathcal{X}_{2l+1}\right). \tag{10}$$

Thus the interlayer interaction is determined by the interlayer susceptibility. We proceed with the evaluation of the normal and superconducting contributions to this key quantity.

III. NORMAL-STATE INTERLAYER SUSCEPTIBILITY

The indirect interaction between localized magnetic moments in metals mediated by conducting electrons is known as the RKKY interaction [18]. Its shape is determined by the nonlocal spin susceptibility, which in the standard case of closed Fermi surface has a well-known oscillating behavior $\propto -\cos(2p_{F,r}r)/r^3$, where $p_{F,r}$ is the Fermi momentum along the considered direction[56]. The behavior for a layered material with the spectrum in Eq. (3) corresponding to open Fermi surface is qualitatively different. In this case the spin susceptibility $\chi_n(\boldsymbol{r})$ in Eqs. (6) and (8) is

$$\begin{aligned} \chi_n(\boldsymbol{r}) = -2\int\frac{d^2\boldsymbol{p}dq}{(2\pi)^3}\int\frac{d^3\boldsymbol{p}'dq'}{(2\pi)^3}\frac{f(\boldsymbol{p},q)-f(\boldsymbol{p}',q')}{\varepsilon(\boldsymbol{p},q)-\varepsilon(\boldsymbol{p}',q')} \\ \times\exp\left[i\left(\boldsymbol{p}-\boldsymbol{p}'\right)\boldsymbol{r}+i\left(q-q'\right)n\right], \end{aligned} \tag{11}$$

where $f(\boldsymbol{p},q) = \{1+\exp[(\varepsilon(\boldsymbol{p},q)-\varepsilon_F)/T]\}^{-1}$ is the Fermi-Dirac distribution function and the energy $\varepsilon(\boldsymbol{p},q)$ is given by Eq. (3). The nonlocal susceptibility of layered metal has been evaluated in Ref. [57]. It oscillates both as a function of $\boldsymbol{r}$ at fixed n and as a function of layer index n at fixed $\boldsymbol{r}$. Here we reconsider this problem with the goal to directly evaluate the interlayer susceptibility in Eq. (8). Using the above formula for $\chi_n(\boldsymbol{r})$, we derive the convenient representation

$$\begin{aligned} \mathcal{X}_n^N = -\int_{-\pi}^{\pi}\frac{dq}{2\pi}\int_{-\pi}^{\pi}\frac{dq'}{2\pi}\int d\xi\nu_{2D}(\xi) \\ \times\frac{f(\xi+\varepsilon_z)-f(\xi+\varepsilon_z')}{\varepsilon_z-\varepsilon_z'}\exp\left[i\left(q-q'\right)n\right], \end{aligned} \tag{12}$$

where

$$\nu_{2D}(\xi) = 2\int\frac{d^2\boldsymbol{p}}{(2\pi)^2}\delta\left(\xi-\varepsilon_{2D}\left(\boldsymbol{p}\right)+\varepsilon_F\right) \tag{13}$$

is the total density of states for an isolated layer for both spin orientations, $f(\xi) = [1+\exp(\xi/T)]^{-1}$, and we use

[1] The effective exchange field caused by nonuniform magnetic field $\boldsymbol{H}(\boldsymbol{r})$ is $\boldsymbol{h}(\boldsymbol{r}) = \mu_0\boldsymbol{H}(\boldsymbol{r})$, where μ_0 is the electron's magnetic moment

the abbreviations $\varepsilon_z = \varepsilon_z(q)$ and $\varepsilon'_z = \varepsilon_z(q')$. We will be mostly interested in the zero-temperature limit for which we obtain

$$\mathcal{X}_n^N = -\int_{-\pi}^{\pi}\frac{dq}{2\pi}\int_{-\pi}^{\pi}\frac{dq'}{2\pi}\int_{-\varepsilon'_z}^{-\varepsilon_z} d\xi \frac{\nu_{2D}(\xi)}{\varepsilon_z - \varepsilon'_z}\exp\left[i\left(q-q'\right)n\right]. \quad (14)$$

Note that the sum $\sum_{n=-\infty}^{\infty}\mathcal{X}_n^N$ gives the uniform susceptibility equal to $\nu_{2D}(0)$.

For quadratic in-layer spectrum, we have the well-known energy-independent 2D DoS $\nu_{2D}(\varepsilon, q) = m/\pi$. In this case the above equation immediately gives $\mathcal{X}_n^N = \nu_{2D}\delta_n$, i.e., *for the quadratic spectrum the RKKY interaction between ferromagnetically-ordered layers is absent.* The oscillating coordinate dependence of $\chi_n(\boldsymbol{r})$ has been evaluated in Ref. [57]. It is crucial that the integral of this function over $\boldsymbol{r}$ vanishes for $n \neq 0$ and this property has important implications for the RKKY interaction between ferromagnetically-ordered layers.

In general, the density of state is energy dependent. When variation of $\nu_{2D}(\xi)$ at the scale $\xi \sim \varepsilon_z$ are weak, we can use expansion with respect to derivatives of $\nu_{2D}(\xi)$ near the Fermi level

$$\int_{-\varepsilon'_z}^{-\varepsilon_z} d\xi \nu_{2D}(\xi) = \sum_{s=0}^{\infty}\nu_{2D}^{(s)}\frac{(-\varepsilon_z)^{s+1} - (-\varepsilon'_z)^{s+1}}{(s+1)!},$$

with $\nu_{2D}^{(s)} \equiv d^s\nu_{2D}/d\xi^s$ at $\xi = 0$, which yields

$$\mathcal{X}_n^N = \sum_{s=0}^{\infty}\frac{(-1)^s\nu_{2D}^{(s)}}{(s+1)!} \times \int_{-\pi}^{\pi}\frac{dq}{2\pi}\int_{-\pi}^{\pi}\frac{dq'}{2\pi}\frac{\varepsilon_z^{s+1} - \varepsilon_z'^{s+1}}{\varepsilon_z - \varepsilon'_z}\exp\left[i\left(q-q'\right)n\right].$$

The second-derivative term ($s=2$) in this sum,

$$\frac{\nu''_{2D}}{6}\left(2\delta_n\int_{-\pi}^{\pi}\frac{dq}{2\pi}\varepsilon_z^2 + \left|\int_{-\pi}^{\pi}\frac{dq}{2\pi}\varepsilon_z\exp\left(iqn\right)\right|^2\right),$$

gives a finite nearest-neighbor interlayer interaction. For $\varepsilon_z = -2t_\perp\cos q$, we have $\int_{-\pi}^{\pi}\frac{dq}{2\pi}\varepsilon_z\exp\left(iqn\right) = -t_\perp\delta_{|n|-1}$ and

$$\mathcal{X}_1^N \approx \frac{\nu''_{2D}}{6}t_\perp^2. \quad (15)$$

The interaction is ferromagnetic if $\nu''_{2D} > 0$. As $\nu''_{2D} \approx \nu_{2D}/W^2$, where W is the in-plane band width, $\mathcal{X}_1^N \sim \mathcal{X}_0^N t_\perp^2/W^2 \ll \mathcal{X}_0$. For larger n, $\mathcal{X}_n^N$ steeply decreases as $\mathcal{X}_0^N\left(t_\perp^2/W^2\right)^n$ meaning that the terms with $n > 1$ can be safely neglected. Such behavior is very different from the conventional oscillating behavior with the power envelope decrease, which is realized for closed Fermi surfaces.

For example, for the quartic correction to the spectrum in the form

$$\varepsilon_{\boldsymbol{p}}^{(2D)} = \frac{p^2}{2m} + \frac{\alpha\left(p_x^4 + p_y^4\right)}{4m^2} \quad (16)$$

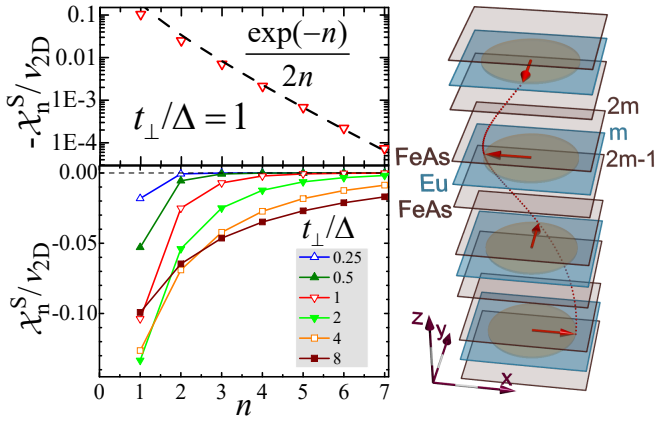

FIG. 1. Lower left: The plots of the superconducting contribution to the interlayer susceptibility $\mathcal{X}_n^S$ normalized to DoS ν_{2D}, Eq. (20), for different ratios $t_\perp/\Delta$. The upper left figure shows the semilog plot of $-\mathcal{X}_n^S/\nu_{2D}$ for $t_\perp/\Delta = 1$ together with the analytical large-n asymptotics. The picture on the right illustrates the arrangement of the magnetic Eu and conducting FeAs layers in $RbEuFe_4As_4$ and the interlayer helical magnetic order.

the density of states is

$$\nu_{2D}(\xi) = \frac{m}{\pi}\int_0^\pi\frac{d\theta}{\pi}\frac{1}{\sqrt{1+\alpha(\varepsilon_F+\xi)\left(3+\cos\theta\right)}}.$$

The expansion for small ξ valid for $\alpha\varepsilon_F \ll 1$ gives

$$\nu''_{2D} \approx \frac{m}{\pi}\frac{57}{8}\alpha^2. \quad (17)$$

In this case $\nu''_{2D} > 0$ meaning that the spectrum in Eq. (16) favors the ferromagnetic alignment between the layers, independently of sign of the quartic coefficient α.

IV. SUPERCONDUCTING CONTRIBUTION TO INTERLAYER SUSCEPTIBILITY

We proceed with evaluation of the superconducting contribution to the interlayer susceptibility. A general formula for the nonlocal spin susceptibility in the superconducting state is

$$\chi(\boldsymbol{r}, n) = -2T\sum_{\omega_s}\left[\mathcal{G}^2\left(\omega_s, \boldsymbol{r}, n\right) + \left|\mathcal{F}\left(\omega_s, \boldsymbol{r}, n\right)\right|^2\right], \quad (18)$$

see, e.g., Ref. [58]. Here $\omega_s = \pi T(2s+1)$ are the Matsubara frequencies,

$$\mathcal{G}\left(\omega_s, \boldsymbol{r}, n\right) = \int_{\boldsymbol{p},q}\exp\left(i\boldsymbol{p}\boldsymbol{r} + iqn\right)\frac{i\omega_s + \xi(\boldsymbol{p}, q)}{\omega_s^2 + \left[\xi(\boldsymbol{p}, q)\right]^2 + \Delta^2},$$
$$\mathcal{F}\left(\omega_s, \boldsymbol{r}, n\right) = \int_{\boldsymbol{p},q}\exp\left(i\boldsymbol{p}\boldsymbol{r} + iqn\right)\frac{\Delta}{\omega_s^2 + \left[\xi(\boldsymbol{p}, q)\right]^2 + \Delta^2}$$

are the regular and anomalous Green's functions with $\int_{\boldsymbol{p},q} \equiv \int\frac{d^2\boldsymbol{p}}{(2\pi)^2}\int_{-\pi}^{\pi}\frac{dq}{2\pi}$, and Δ is the superconducting gap.

Therefore, the interlayer susceptibility, Eq. (8), is given by

$$\mathcal{X}_n = -2T\sum_{\omega_s}\int d\boldsymbol{r}\left[\mathcal{G}^2(\omega_s,\boldsymbol{r},n)+\left|\mathcal{F}(\omega_s,\boldsymbol{r},n)\right|^2\right]. \quad (19)$$

Note that the linear response with respect to the effective field h assumed in derivation of Eqs. (6)–(9) is valid for $h \ll \Delta$. We consider again the case of open Fermi surface described by the spectrum $\xi(\boldsymbol{p},q) = p^2/2m + \varepsilon_z(q) - \varepsilon_F$. The derivations described in Appendix A lead to the following presentation for the superconducting contribution to $\mathcal{X}_n$

$$\mathcal{X}_n^S = \nu_{2D}\,\mathcal{S}_n(2t_\perp/\Delta), \quad (20)$$

$$\mathcal{S}_n(\tau) = -\int_0^\pi \frac{dq_+}{\pi}\int_0^\pi \frac{dq_-}{\pi}\cos(q_- n) \times \frac{\ln\left(\sqrt{1+\tau^2\sin^2 q_+\sin^2\left(\frac{q_-}{2}\right)}+\tau\sin q_+\sin\left(\frac{q_-}{2}\right)\right)}{\tau\sin q_+\sin\left(\frac{q_-}{2}\right)\sqrt{1+\tau^2\sin^2 q_+\sin^2\left(\frac{q_-}{2}\right)}}$$

with $\tau \equiv 2t_\perp/\Delta$. Note that, in contrast to the normal state considered in the previous section, the interlayer susceptibility $\mathcal{X}_n^S$ is finite for the quadratic in-layer spectrum corresponding to the energy-independent DoS. It has the negative sign leading to antiferromagnetic interactions between the magnetic layers. The sum $\sum_{n=-\infty}^{\infty}\mathcal{X}_n^S = -\nu_{2D}$ meaning that for the total interlayer susceptibility we have $\sum_{n=-\infty}^{\infty}\left(\mathcal{X}_n^S+\mathcal{X}_n^N\right) = 0$. This is the well-known result for vanishing uniform spin susceptibility in the superconducting state. In the range $\tau \ll 1$, we obtain $\mathcal{X}_n^S/\nu_{2D} = -\left(1-\frac{1}{6}\tau^2\right)\delta_n - \frac{1}{12}\tau^2\delta_{|n|-1}$. Therefore, in the limit of weak tunneling, $t_\perp \ll \Delta$, $\mathcal{X}_n^S$ is only sizable for the nearest neighbors, $n = 1$, as for the normal part, and $|\mathcal{X}_1^S| \propto (t_\perp/\Delta)^2\nu_{2D} \ll \mathcal{X}_0$. On the other hand, $\mathcal{X}_n^S$ has a nonmonotonic dependence on $t_\perp/\Delta$. For example, the absolute value of $\mathcal{X}_1^S$ reaches maximum at $t_\perp \approx 2.4\Delta$. The plots of $\mathcal{X}_n^S/\nu_{2D}$ for several values of $t_\perp/\Delta$ are shown in Fig. 1 (lower left).

The asymptotics at large n

$$\mathcal{X}_n^S \approx -\nu_{2D}\frac{\exp\left(-\frac{\Delta}{t_\perp}n\right)}{2n}, \quad (21)$$

is also evaluated in the Appendix A. This asymptotics is compared with the exact dependence for $t_\perp = \Delta$ in the upper left plot in Fig. 1. Note that the ratio $t_\perp/\Delta$ is approximately equal to the ratio of the c-axis coherence length and the interlayer period. We see that in the case $t_\perp \gtrsim \Delta$ superconductivity introduces the long-range interaction between the magnetic layers. Such behavior is unique for the interlayer RKKY interaction between ferromagnetic layers.

V. GENERALIZATION TO MULTIPLE-BAND MATERIAL

The Fermi surface of iron pnictides is composed of several holelike sheets near the Brillouin-zone center and electronlike sheets at the Brillouin-zone edge. The bands crossing the Fermi level are mostly composed from the iron d-orbitals. The corresponding Fermi surfaces are typically open, except near the Lifshitz transitions. In the case of hole-doped 1144 materials, the band-structure calculations suggest that six hole bands and four electron bands cross the Fermi level [59, 60].

The results of this paper can be straightforwardly generalized to the multiband case. A band with the index j is characterized by set of relevant parameters: hopping integral $t_{\perp,j}$, 2D density of states $\nu_{2D,j}$, superconducting gap Δ_j, and exchange interaction with the local moments $\mathcal{J}_{j,nm}$. The gap parameters in the electron and hole bands may have opposite signs ($s_\pm$ state). This feature has no influence of the phenomena studied in this paper and Δ_j notate the absolute values of the gaps. The interlayer RKKY interactions in Eq. (9) can be obtained by the summation of the band contributions,

$$\mathcal{I}_{m-m'} = \sum_j\sum_{n,n'}\mathcal{X}_{j,n-n'}\mathcal{J}_{j,nm}\mathcal{J}_{j,n'm'}. \quad (22)$$

The normal and superconducting contributions to the partial interlayer susceptibilities $\mathcal{X}_{j,n}$ are similar to the corresponding single-band results in Eqs. 15 and (20)

$$\mathcal{X}_{j,1}^N \approx \frac{\nu''_{2D,j}}{6}t_{\perp,j}^2, \quad \mathcal{X}_{j,n}^S = \nu_{2D,j}\mathcal{S}_n(2t_{\perp,j}/\Delta_j),$$

where the function $\mathcal{S}_n(\tau)$ is defined in Eq. (20). As these components are controlled by very different electronic parameters, the dominating contributions to the normal and superconducting parts of $\mathcal{I}_{m-m'}$ may come from different bands. For more complicated interlayer tunneling mechanisms, the z-axis spectrum $\varepsilon_{z,j}$ may have non-cosine form and depend on the in-plane momentum $\boldsymbol{p}$. In this case the parameter $t_{\perp,j}$ in the above equations has to be replaced with $\left\langle\left|\int_{-\pi}^{\pi}\frac{dq}{2\pi}\varepsilon_{z,j}(\boldsymbol{p}_{F,j},q)\exp(iq)\right|^2\right\rangle^{1/2}$, where the averaging has to be taken over the in-plane Fermi momentum $\boldsymbol{p}_{F,j}$.

As the normal contribution to the interlayer susceptibility is ferromagnetic and short-range and the superconducting contribution is antiferromagnetic and long-range for $t_{\perp,j} > \Delta_j$, the interactions between the magnetic layers are frustrated. This is the main reason for the formation of the helical magnetic structures considered in the next section.

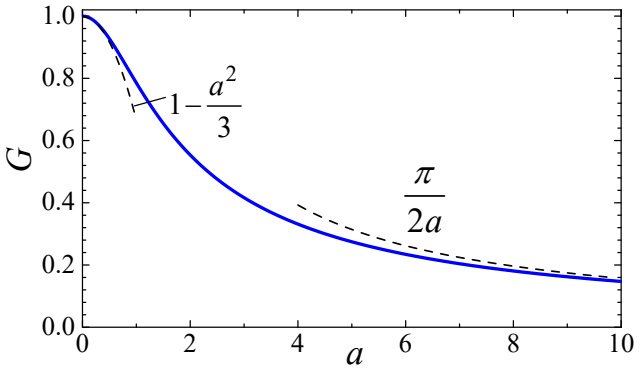

FIG. 2. The plot of the function $G(a)$ defined by Eq. (27), which determines the dependence of the superconducting interlayer energy on the modulation wave vector Q, Eq. (26).

VI. ENERGY OF INTERLAYER HELICAL STRUCTURE

We consider the magnetic structure in the form of a helix

$$\left\langle S_m^X \right\rangle = S_0 \cos\left(Qm\right), \left\langle S_m^Y \right\rangle = S_0 \sin\left(Qm\right), \left\langle S_m^Z \right\rangle = 0.$$

In this case the interlayer-interaction energy, Eq. (7), becomes

$$F_{\rm h}(Q) = -S_0^2 \sum_{l=1}^{\infty} \mathcal{I}_l \cos\left(Ql\right). \tag{23}$$

As this work is motivated by the magnetic 1144 iron arsenides, we now evaluate the energy of helical structure for layer's arrangement realized in these compounds illustrated in Fig. 1. In this case, the relation between the interlayer exchange interaction $\mathcal{I}_l$ and interlayer susceptibility $\mathcal{X}_n$ is given by Eq. (10). For illustration, we consider here a single-band case. As discussed in the previous section, generalization to multiple bands is straightforward. In the normal state, we can take into account only the nearest-neighbor interlayer susceptibility $\mathcal{X}_1^N$ yielding

$$\mathcal{I}_1^N \approx \mathcal{J}^2 \mathcal{X}_1^N,$$

where $\mathcal{X}_1^N$ is given by Eq. (15). Therefore, the normal contribution to the energy, Eq. (23) is

$$F_{\rm h}^N(Q) \approx -h_0^2 \mathcal{X}_1^N \cos Q, \tag{24}$$

where

$$h_0 = \mathcal{J} S_0 \tag{25}$$

is the amplitude of exchange field induced by polarized magnetic ions on the conducting electrons.

The derivation of the superconducting contribution is outlined in Appendix B and leads to the following result

$$F_{\rm h}^S(Q) = \frac{\nu_{2D}}{2} h_0^2 \left\{ \left(1+\cos\frac{Q}{2}\right) G\left[\frac{2t_\perp}{\Delta}\sin\frac{Q}{4}\right] + \left(1-\cos\frac{Q}{2}\right) G\left[\frac{2t_\perp}{\Delta}\cos\frac{Q}{4}\right] \right\} \tag{26}$$

with the reduced function

$$G\left(a\right) = \frac{1}{a}\int_0^\pi \frac{dq}{\pi} \frac{\ln\left(\sqrt{a^2\sin^2 q + 1} + a\sin q\right)}{\sin q \sqrt{a^2 \sin^2 q + 1}}, \tag{27}$$

which is plotted in Fig. 2. This function has the following asymptotics

$$G\left(a\right) \simeq \begin{cases} 1 - \frac{1}{3}a^2, & \text{for } a \ll 1 \\ \frac{\pi}{2a}, & \text{for } a \gg 1 \end{cases},$$

also shown in the plot. Independently on the relation between $t_\perp$ and Δ, $F_{\rm h}^S(Q)$ monotonically decreases with increasing Q indicating that the superconducting contribution by itself favors the maximum possible modulation vector $Q = \pi$. In two limiting cases, we obtain

$$F_{\rm h}^S(Q) \simeq \frac{\nu_{2D}}{2} h_0^2 \times \begin{cases} 2 - \frac{1}{3}\frac{4t_\perp^2}{\Delta^2}\sin^2\frac{Q}{2}, & \text{for } \frac{2t_\perp}{\Delta} \ll 1 \\ \frac{\pi}{2}\frac{\Delta}{t_\perp}\left(\cot\frac{Q}{4}\cos\frac{Q}{4} + \tan\frac{Q}{4}\sin\frac{Q}{4}\right), & \text{for } \frac{2t_\perp}{\Delta}\sin\frac{Q}{4} \gg 1 \end{cases}. \tag{28}$$

In the case $t_\perp \gg \Delta$, the superconducting contribution increases $\propto 1/Q$ with decreasing Q in the range $\Delta/t_\perp \ll Q \ll 1$, similar to the isotropic case [22]. We proceed with evaluation of the optimal modulation wave vector from the derived energy of the helical state, $F_{\rm h}(Q) = F_{\rm h}^N(Q) + F_{\rm h}^S(Q)$.

VII. OPTIMAL MODULATION WAVE VECTOR

The helical structures with the modulation wave vector in the range $0 < Q < \pi$ may realize only if the interlayer hopping $t_\perp$ is either comparable with or larger than the gap Δ. We limit ourselves to the analy-

sis of the case $t_\perp \gg \Delta$. In addition to the normal and superconducting RKKY contributions considered in the previous sections, the ground-state configuration of the localized moments is also affected by the in-plane four-fold anisotropy described by the single-spin energy $-K_4\left(S_x^4+S_y^4\right)$. For a simple helical structure this gives the contribution to the energy per layer and per unit area, $-\mathcal{K}_4\left\langle\cos^4(Qm)+\sin^4(Qm)\right\rangle_m = -\frac{\mathcal{K}_4}{4}\left(3+\left\langle\cos(4Qm)\right\rangle_m\right)$, where $\mathcal{K}_4 = K_4 S_0^4 n_M$ and n_M is the moment's density per unit area. Therefore we can write the energy of the helical structure as

$$F_{\rm h}(Q) = -\mathcal{A}_N\cos Q + \mathcal{A}_S\frac{\cos^3\left(\frac{Q}{4}\right)+\sin^3\left(\frac{Q}{4}\right)}{\sin\left(\frac{Q}{4}\right)\cos\left(\frac{Q}{4}\right)} - \frac{\mathcal{K}_4}{4}\left\langle\cos(4Qm)\right\rangle_m \tag{29}$$

with $\mathcal{A}_N \approx \frac{1}{6}h_0^2\nu''_{2D}t_\perp^2$ and $\mathcal{A}_S = \frac{\pi}{4}h_0^2\nu_{2D}\frac{\Delta}{t_\perp}$ following from the previous-section results (for multiple-band case, $\mathcal{A}_N \approx \frac{1}{6}S_0^2\sum_j \mathcal{J}_j^2\nu''_{2D,j}t_{\perp,j}^2$ and $\mathcal{A}_S = \frac{\pi}{4}S_0^2\sum_j \mathcal{J}_j^2\nu_{2D,j}\frac{\Delta_j}{t_{\perp,j}}$). Within this simple model, the anisotropic contribution is only finite for $Q=\pi/2$ and π. Without the anisotropy term, the optimal modulation vector Q_o continuously changes as function of the ratio $\mathcal{A}_S/\mathcal{A}_N$. In the presence of the four-fold anisotropy, Q_o is locked to the values $\pi/2$ and π within finite ranges of $\mathcal{A}_S/\mathcal{A}_N$. These ranges can be approximately estimated by comparison the energies of commensurate and incommensurate configurations.

For incommensurate structures with optimal modulation wave vector $Q_o \neq \pi/2, \pi$, the ground-state energy is

$$F_{\rm h}(Q_o) = \mathcal{A}_N \min_Q\left[-\cos Q + \frac{\mathcal{A}_S}{\mathcal{A}_N}\frac{\cos^3\left(\frac{Q}{4}\right)+\sin^3\left(\frac{Q}{4}\right)}{\sin\left(\frac{Q}{4}\right)\cos\left(\frac{Q}{4}\right)}\right] \tag{30}$$

where, in a single-band case,

$$\frac{\mathcal{A}_S}{\mathcal{A}_N} = \frac{3\pi}{2}\frac{\nu_{2D}\Delta}{\nu''_{2D}t_\perp^3}. \tag{31}$$

On the other hand, the energies for $Q_o=\pi/2$ and π are

$$F_{\rm h}(\pi/2) = C_{\pi/2}\mathcal{A}_S - \frac{\mathcal{K}_4}{4} \tag{32}$$

$$F_{\rm h}(\pi) = \mathcal{A}_N + \frac{\mathcal{A}_S}{\sqrt{2}} - \frac{\mathcal{K}_4}{4} \tag{33}$$

with $C_{\pi/2} = (1+1/\sqrt{2})^{3/2}+(1-1/\sqrt{2})^{3/2} \approx 2.39$.

Figure 3 shows the phase diagram following from comparison of the energies in Eqs. (30), (32) and (33). We see that the modulation vector increases with increasing the ratio $\mathcal{A}_S/\mathcal{A}_N$, and at finite $\mathcal{K}_4$ the commensurate states are realized within finite ranges of $\mathcal{A}_S/\mathcal{A}_N$. In particular, at $\mathcal{K}_4=0$ the $\pi/2$ helix is realized at $\mathcal{A}_S/\mathcal{A}_N \approx 0.625$ and the range of $\mathcal{A}_S/\mathcal{A}_N$, where this phase is locked rapidly

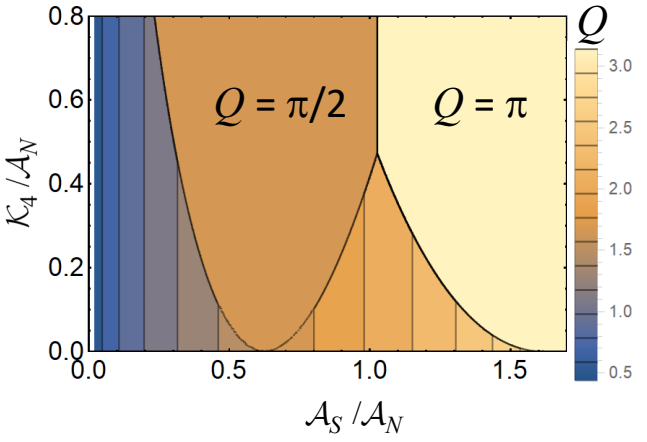

FIG. 3. Phase diagram for helical structures in layered magnetic superconductors in the plane $\mathcal{A}_S/\mathcal{A}_N$–$\mathcal{K}_4/\mathcal{A}_N$, where the first ratio is given by Eq. (31). This diagram is computed for the layer arrangement corresponding to $RbEuFe_4As_4$, see inset in Fig. 2, and for the case $t_\perp \gg \Delta$.

increases with increasing $\mathcal{K}_4$. Note that a simple energy comparison only gives an approximate location of the lines, because in the vicinity of transition a helix does not give the ground state. Consequently, the energy comparison gives somewhat larger extent of the commensurate states. The actual transition from commensurate to incommensurate state occurs via formation of the soliton lattice [61, 62]. The detailed investigation of transitions is beyond the scope of this paper.

VIII. SUMMARY AND DISCUSSION

In conclusion, we investigated the interlayer RKKY interactions and equilibrium magnetic structure for a material composed of superconducting and ferromagnetic layers in the situation when the finite coupling between the magnetic layers is mediated by tunneling between the conducting layers. We demonstrated that for a shallow band with the weakly-nonparabolic spectrum, the normal-state contribution to the interlayer RKKY interaction is ferromagnetic and short-range. On the other hand, the superconducting part is antiferromagnetic and may be long-range if the hopping integral exceeds the superconducting gap. As a result of the competition between these two contributions, the ground-state magnetic configuration may be a spiral, similar to isotropic case [22]. On the phenomenological level, the mechanism of the spiral formation is the same as in the Heisenberg model with frustrating exchange interactions, see, e.g., Refs. [63, 64]. Our model provides a natural physical mechanism for such a frustration. In absence of the anisotropy with respect to in-plane rotations of the magnetic moments, the angle between them in the neighboring layers would depend continuously on the model parameters. The finite four-fold moment-rotation

anisotropy may lock this angle to 90°, as it was observed in $RbEuFe_4As_4$.

The superconducting transition in $RbEuFe_4As_4$ sinks below the magnetic transition with increasing pressure[49, 50]. Our model predicts the ferromagnetic alignment of Eu moments in the normal state. Therefore, establishing the magnetic structure in the normal state at high pressures provides an essential test for the model.

Our minimum model does not capture a complicated multiple-band structure of $RbEuFe_4As_4$ obtained by *ab initio* calculations[51, 60]. This calculation suggest that six hole bands and four electron bands cross the Fermi level. All Fermi surfaces are open, in spite of noticeable variations the electronic parameters between the bands. The straightforward generalization of the model to the case of multiple open Fermi surfaces is discussed in Sec. V. Unfortunately, the DFT-based band-structure calculations still have large inaccuracies. For example, the normal-state specific heat coefficient calculated in Ref. [60] is $\sim$ 5-6 times smaller than the experimental value, most likely due to the correlation effects. Do to these inaccuracies and lack of direct experimental information, the relevant parameters can only estimated very approximately: the interlayer hopping $t_\perp = 10-40$ meV, in-layer band width $W = 0.2 - 1$ meV, gap parameter $\Delta = 2 - 10$ meV, and the exchange-field amplitude $h_0 = S_0\mathcal{J} = 0.5 - 1$ meV. Due to such large uncertainties, the quantitative analysis does not look feasible yet. Our consideration only illustrates an essential physical mechanism responsible for the formation of the spiral magnetic structure in $RbEuFe_4As_4$ and similar materials and provides the basis for more realistic descriptions.

ACKNOWLEDGMENTS

I would like to thank U. Welp, Z. Islam, O. Chmaissem, and S. Rosenkranz for discussions of experimental data and physics of the magnetic iron arsenides. This work was supported by the US Department of Energy, Office of Science, Basic Energy Sciences, Materials Sciences and Engineering Division.

Appendix A: Derivation of interlayer susceptibility in superconducting state

In this appendix we present the derivation details for the susceptibility integrated over in-plane coordinates, Eqs. (8) and (19). Using the presentation

$$\int d\boldsymbol{r}\mathcal{G}^2\left(\omega_s,\boldsymbol{r},n\right)=\int\frac{d^2\boldsymbol{p}}{(2\pi)^2}\mathcal{G}^2\left(\omega_s,\boldsymbol{p},n\right)=\int d\xi\nu_{2D}(\xi)\int_{-\pi}^{\pi}\frac{dq}{2\pi}\int_{-\pi}^{\pi}\frac{dq'}{2\pi}\mathcal{G}\left(\omega_s,\xi,q\right)\mathcal{G}\left(\omega_s,\xi,-q'\right)\exp\left[i\left(q-q'\right)n\right]$$

with

$$\mathcal{G}\left(\omega_s,\xi,q\right)=\frac{i\omega_s+\xi+\varepsilon_z(q)}{\omega_s^2+\left[\xi+\varepsilon_z(q)\right]^2+\Delta^2},$$

and similar presentation for the anomalous part $\int d\boldsymbol{r}\mathcal{F}^2\left(i\omega_s,\boldsymbol{r},n\right)$, we transform $\mathcal{X}_n$ in Eq. (19) to

$$\mathcal{X}_n=-\int d\xi\nu_{2D}(\xi)\int_{-\pi}^{\pi}\frac{dq}{2\pi}\int_{-\pi}^{\pi}\frac{dq'}{2\pi}\exp\left[i\left(q-q'\right)n\right]\mathcal{R}\left[\xi+\varepsilon_z(q),\xi+\varepsilon_z(q')\right],$$

where

$$\mathcal{R}\left(\varsigma,\varsigma'\right)=-T\sum_{\omega_s}\frac{\omega_s^2-\varsigma\varsigma'-\Delta^2}{\left(\omega_s^2+\varsigma^2+\Delta^2\right)\left(\omega_s^2+\varsigma'^2+\Delta^2\right)}.$$

Performing summation over ω_s, we obtain

$$\mathcal{R}\left(\varsigma,\varsigma'\right)=-\frac{1}{2\left(\varsigma^2-\varsigma'^2\right)}\left[\frac{\varsigma^2+\varsigma\varsigma'+2\Delta^2}{\sqrt{\varsigma^2+\Delta^2}}\tanh\left(\frac{\sqrt{\varsigma^2+\Delta^2}}{2T}\right)-\frac{\varsigma'^2+\varsigma\varsigma'+2\Delta^2}{\sqrt{\varsigma'^2+\Delta^2}}\tanh\left(\frac{\sqrt{\varsigma'^2+\Delta^2}}{2T}\right)\right],$$

where we used $T\sum_{\omega_s}\frac{1}{\omega_s^2+z^2}=\frac{\tanh(z/2T)}{2z}$. In the limit $T\to 0$

$$\mathcal{R}\left(\varsigma,\varsigma'\right)=-\frac{1}{2\left(\sqrt{\varsigma^2+\Delta^2}+\sqrt{\varsigma'^2+\Delta^2}\right)}\left[1-\frac{\varsigma\varsigma'+\Delta^2}{\sqrt{\varsigma^2+\Delta^2}\sqrt{\varsigma'^2+\Delta^2}}\right].$$

Therefore, at $T=0$ we obtain

$$\mathcal{X}_n = \int d\xi \nu_{2D}(\xi) \int\limits_{-\pi}^{\pi} \frac{dq}{2\pi} \int\limits_{-\pi}^{\pi} \frac{dq'}{2\pi} \frac{\exp\left[i\left(q-q'\right)n\right]}{2\left(\sqrt{\left(\xi+\varepsilon_z\right)^2+\Delta^2}+\sqrt{\left(\xi+\varepsilon_z'\right)^2+\Delta^2}\right)} \left[1-\frac{\left(\xi+\varepsilon_z\right)\left(\xi+\varepsilon_z'\right)+\Delta^2}{\sqrt{\left(\xi+\varepsilon_z\right)^2+\Delta^2}\sqrt{\left(\xi+\varepsilon_z'\right)^2+\Delta^2}}\right]$$

where we use abbreviations $\varepsilon_z = \varepsilon_z(q)$ and $\varepsilon_z' = \varepsilon_z(q')$. This result is consistent with the general presentation for susceptibility derived in the Abrikosov book [13], Eq. (21.44). Subtracting the normal part for $\Delta = 0$, we obtain the superconducting contribution

$$\mathcal{X}_n^S = \int d\xi \nu_{2D}(\xi) \int\limits_{-\pi}^{\pi} \frac{dq}{2\pi} \int\limits_{-\pi}^{\pi} \frac{dq'}{2\pi} \exp\left[i\left(q-q'\right)n\right] \left\{ \frac{1}{2\left(\sqrt{\left(\xi+\varepsilon_z\right)^2+\Delta^2}+\sqrt{\left(\xi+\varepsilon_z'\right)^2+\Delta^2}\right)} \right.$$
$$\left. \times \left[1-\frac{\left(\xi+\varepsilon_z\right)\left(\xi+\varepsilon_z'\right)+\Delta^2}{\sqrt{\left(\xi+\varepsilon_z\right)^2+\Delta^2}\sqrt{\left(\xi+\varepsilon_z'\right)^2+\Delta^2}}\right] - \frac{1-\operatorname{sign}\left(\xi+\varepsilon_z\right)\operatorname{sign}\left(\xi+\varepsilon_z'\right)}{2\left(\left|\xi+\varepsilon_z\right|+\left|\xi+\varepsilon_z'\right|\right)} \right\}.$$

We remind that the normal part vanishes for energy-independent DoS at $n \neq 0$. The superconducting contribution, however, remains finite allowing us to neglect DoS energy dependence in it which yields

$$\mathcal{X}_n^S = \nu_{2D} \int\limits_{-\pi}^{\pi} \frac{dq}{2\pi} \int\limits_{-\pi}^{\pi} \frac{dq'}{2\pi} \int d\xi \exp\left[i\left(q-q'\right)n\right] \left\{ \frac{1}{2\left(\sqrt{\left(\xi+\frac{\varepsilon_{z-}}{2}\right)^2+\Delta^2}+\sqrt{\left(\xi-\frac{\varepsilon_{z-}}{2}\right)^2+\Delta^2}\right)} \right.$$
$$\left. \times \left[1-\frac{\xi^2-\varepsilon_{z-}^2/4+\Delta^2}{\sqrt{\left(\xi+\frac{\varepsilon_{z-}}{2}\right)^2+\Delta^2}\sqrt{\left(\xi-\frac{\varepsilon_{z-}}{2}\right)^2+\Delta^2}}\right] - \frac{\Theta\left(\frac{\left|\varepsilon_{z-}\right|}{2}-\xi\right)}{\left|\varepsilon_{z-}\right|} \right\}. \tag{A1}$$

with $\varepsilon_{z-} = \varepsilon_z - \varepsilon_z'$. Making substitution $\xi = \frac{\varepsilon_{z-}}{2}x$, we present the dimensionless ratio $\mathcal{X}_n^S/\nu_{2D}$ as

$$\mathcal{X}_n^S/\nu_{2D} = \int_{-\pi}^{\pi} \frac{dq}{2\pi} \int_{-\pi}^{\pi} \frac{dq'}{2\pi} \exp\left[i\left(q-q'\right)n\right] G[2\Delta/|\varepsilon_{z-}|],$$
$$G[a] = \frac{1}{2} \int\limits_{-\infty}^{\infty} dx \left\{ \left[1-\frac{x^2-1+a^2}{\sqrt{\left(x+1\right)^2+a^2}\sqrt{\left(x-1\right)^2+a^2}}\right] \frac{1}{\sqrt{\left(x+1\right)^2+a^2}+\sqrt{\left(x-1\right)^2+a^2}} - \Theta(1-|x|) \right\}$$
$$= -\frac{a^2}{\sqrt{a^2+1}} \ln\left(\frac{\sqrt{a^2+1}+1}{a}\right).$$

This gives a useful presentation

$$\frac{\mathcal{X}_n^S}{\nu_{2D}} = -\int_{-\pi}^{\pi} \frac{dq}{2\pi} \int_{-\pi}^{\pi} \frac{dq'}{2\pi} \exp\left[i\left(q-q'\right)n\right] \frac{2\Delta^2/\left|\varepsilon_{z-}\right|}{\sqrt{\Delta^2+\varepsilon_{z-}^2/4}} \ln\left(\frac{\sqrt{\Delta^2+\varepsilon_{z-}^2/4}+\left|\varepsilon_{z-}\right|/2}{\Delta}\right). \tag{A2}$$

For simple tunneling spectrum $\varepsilon_{z-} = 4t_\perp \sin\left(q_+\right) \sin\left(\frac{q_-}{2}\right)$ with $q_+ = \frac{q+q'}{2}$ and $q_- = q-q'$. This allows us to transform Eq. (A2) to the following form

$$\frac{\mathcal{X}_n^S}{\nu_{2D}} = -\int_0^{\pi} \frac{dq_+}{\pi} \int_0^{\pi} \frac{dq_-}{\pi} \frac{\cos\left(q_- n\right) \ln\left(\sqrt{1+\tau^2\sin^2 q_+ \sin^2\left(\frac{q_-}{2}\right)}+\tau\sin q_+ \sin\left(\frac{q_-}{2}\right)\right)}{\tau\sin q_+ \sin\left(\frac{q_-}{2}\right)\sqrt{1+\tau^2\sin^2 q_+ \sin^2\left(\frac{q_-}{2}\right)}} \tag{A3}$$

with $\tau \equiv 2t_\perp/\Delta$. This result is equivalent to Eq. (20) of the main text. In particular, for $\tau \ll 1$, using expansion $\ln\left(\sqrt{1+x^2}+x\right) \approx x - \frac{1}{6}x^3$, we obtain

$$\frac{\mathcal{X}_n}{\nu_{2D}} = -\left(1-\frac{1}{6}\tau^2\right)\delta_n - \frac{1}{12}\tau^2\delta_{|n|-1}. \tag{A4}$$

Therefore, in the case $t_\perp \ll \Delta$ the superconducting contribution to the RKKY interaction is short-range, similar to the normal part.

The asymptotics at large n is determined by the region $q_- \ll 1$.

$$\frac{\mathcal{X}_n^S}{\nu_{2D}} \approx -\int_0^\pi \frac{dq_+}{\pi}\int_0^\infty \frac{dq_-}{\pi}\cos(q_- n)\,\frac{\ln\left(\sqrt{1+\tau^2\sin^2 q_+\left(\frac{q_-}{2}\right)^2}+\tau\sin q_+\left(\frac{q_-}{2}\right)\right)}{\tau\sin q_+\left(\frac{q_-}{2}\right)\sqrt{1+\tau^2\sin^2 q_+\left(\frac{q_-}{2}\right)^2}}.$$

Making substitution $k=\tau\sin(q_+)\,\frac{q_-}{2}$, we obtain presentation

$$\frac{\mathcal{X}_n^S}{\nu_{2D}} \approx -\frac{2}{\tau\pi}\int_0^\pi \frac{dq_+}{\pi\sin q_+}\mathcal{G}\left(\frac{2}{\tau}\frac{n}{\sin q_+}\right),$$
$$\mathcal{G}(a)=\int_0^\infty dk\cos(ak)\,\frac{\ln\left(\sqrt{1+k^2}+k\right)}{k\sqrt{1+k^2}}.$$

Deforming the integration contour into the complex plane, we obtain

$$\mathcal{G}(a)=\frac{\pi}{2}\int_1^\infty dz\frac{\exp(-az)}{z\sqrt{z^2-1}}\approx\frac{\pi}{2\sqrt{2}}\exp(-a)\int_0^\infty dx\exp(-ax)\,\frac{1}{\sqrt{x}}=\frac{\pi^{3/2}}{2\sqrt{2a}}\exp(-a).$$

Therefore

$$\frac{\mathcal{X}_n^S}{\nu_{2D}} \approx -\frac{1}{2\sqrt{\pi\tau n}}\int_0^\pi\frac{dq_+}{\sqrt{\sin q_+}}\exp\left(-\frac{2}{\tau}\frac{n}{\sin q_+}\right)$$
$$\approx -\frac{\exp\left(-\frac{2}{\tau}n\right)}{2\sqrt{\pi\tau n}}\int_{-\infty}^\infty dx\exp\left(-\frac{n}{\tau}x^2\right)=-\frac{\exp\left(-\frac{2}{\tau}n\right)}{2n}$$

giving the result in Eq. (21).

Appendix B: Derivation of superconducting energy of helical structure

The superconducting contribution to the helical-structure energy, Eq. (23) is

$$F_{\rm h}^S(Q)=-S_0^2\mathcal{J}^2\sum_{l=1}^\infty\sum_{\delta,\delta'=0,1}\mathcal{X}^S_{2l-\delta+\delta'}\cos(Ql), \tag{B1}$$

where $\mathcal{X}_n^S$ is given by Eq. (20). For further simplification, we use the identity

$$\sum_{\delta,\delta'=0,1}\sum_{l=1}^\infty\cos\left[q_-(2l-\delta+\delta')\right]\cos(Ql)=\frac{\pi}{2}(1+\cos q_-)\left\{\sum_{m=-\infty}^\infty\left[\delta(q_-+\frac{Q}{2}-\pi m)+\delta(q_--\frac{Q}{2}-\pi m)\right]-2\right\}.$$

As $0<q_-,Q<\pi$, only nonzero δ-function terms are with $q_-=Q/2$ and $q_-=\pi-Q/2$, which gives the Q-dependent part of energy as

$$F_{\rm h}^S(Q)=\frac{1}{2}\nu_{2D}S_0^2\mathcal{J}^2\int_0^\pi\frac{dq_+}{\pi}\left[\left(1+\cos\frac{Q}{2}\right)\frac{\ln\left(\sqrt{1+\tau^2\sin^2 q_+\sin^2\left(\frac{Q}{4}\right)}+\tau\sin q_+\sin\left(\frac{Q}{4}\right)\right)}{\tau\sin q_+\sin\left(\frac{Q}{4}\right)\sqrt{1+\tau^2\sin^2 q_+\sin^2\left(\frac{Q}{4}\right)}}\right.$$
$$\left.+\left(1-\cos\frac{Q}{2}\right)\frac{\ln\left(\sqrt{1+\tau^2\sin^2 q_+\cos^2\left(\frac{Q}{4}\right)}+\tau\sin q_+\cos\left(\frac{Q}{4}\right)\right)}{\tau\sin q_+\cos\left(\frac{Q}{4}\right)\sqrt{1+\tau^2\sin^2 q_+\cos^2\left(\frac{Q}{4}\right)}}\right]. \tag{B2}$$

This result is equivalent to Eq. (26) in the main text.

[1] Z. Ren, Z. Zhu, S. Jiang, X. Xu, Q. Tao, C. Wang, C. Feng, G. Cao, and Z. Xu, Antiferromagnetic transition in $EuFe_2As_2$: A possible parent compound for supercon-

ductors, Phys. Rev. B **78**, 052501 (2008).
[2] H. S. Jeevan, Z. Hossain, D. Kasinathan, H. Rosner, C. Geibel, and P. Gegenwart, High-temperature superconductivity in $Eu_{0.5}K_{0.5}Fe_2As_2$, Phys. Rev. B **78**, 092406 (2008).
[3] H. S. Jeevan, Z. Hossain, D. Kasinathan, H. Rosner, C. Geibel, and P. Gegenwart, Electrical resistivity and specific heat of single-crystalline $EuFe_2As_2$: A magnetic homologue of $SrFe_2As_2$, Phys. Rev. B **78**, 052502 (2008).
[4] Z. Ren, Q. Tao, S. Jiang, C. Feng, C. Wang, J. Dai, G. Cao, and Z. Xu, Superconductivity induced by phosphorus doping and its coexistence with ferromagnetism in $EuFe_2(As_{0.7}P_{0.3})_2$, Phys. Rev. Lett. **102**, 137002 (2009).
[5] H. S. Jeevan, D. Kasinathan, H. Rosner, and P. Gegenwart, Interplay of antiferromagnetism, ferromagnetism, and superconductivity in $EuFe_2(As_{1-x}P_x)_2$ single crystals, Phys. Rev. B **83**, 054511 (2011).
[6] G. Cao, S. Xu, Z. Ren, S. Jiang, C. Feng, and Z. Xu, Superconductivity and ferromagnetism in $EuFe_2(As_{1-x}P_x)_2$, J. Phys.: Condens. Matter **23**, 464204 (2011).
[7] Y. Liu, Y.-B. Liu, Z.-T. Tang, H. Jiang, Z.-C. Wang, A. Ablimit, W.-H. Jiao, Q. Tao, C.-M. Feng, Z.-A. Xu, and G.-H. Cao, Superconductivity and ferromagnetism in hole-doped $RbEuFe_4As_4$, Phys. Rev. B **93**, 214503 (2016).
[8] Y. Liu, Y.-B. Liu, Q. Chen, Z.-T. Tang, W.-H. Jiao, Q. Tao, Z.-A. Xu, and G.-H. Cao, A new ferromagnetic superconductor: $CsEuFe_4As_4$, Science Bulletin **61**, 1213 (2016).
[9] K. Kawashima, T. Kinjo, T. Nishio, S. Ishida, H. Fujihisa, Y. Gotoh, K. Kihou, H. Eisaki, Y. Yoshida, and A. Iyo, Superconductivity in Fe-based compound $EuAFe_4As_4$ (A = Rb and Cs), J. Phys. Soc. Jpn. **85**, 064710 (2016).
[10] S. Zapf and M. Dressel, Europium-based iron pnictides: a unique laboratory for magnetism, superconductivity and structural effects, Rep. Prog. Phys. **80**, 016501 (2017).
[11] P. Fulde and J. Keller, *Superconductivity in Ternary Compounds II, Superconductivity and Magnetism*, edited by M. B. Maple and Ø. Fischer (Springer, 1982) Chap. 9. Theory of Magnetic Superconductors, pp. 249–294.
[12] L. Bulaevskii, A. Buzdin, M. Kulić, and S. Panjukov, Coexistence of superconductivity and magnetism theoretical predictions and experimental results, Adv. Phys. **34**, 175 (1985).
[13] A. A. Abrikosov, Fundamentals of the theory of metals (North-Holland, 1988) Chap. 21. Superconductivity and Magnetism.
[14] M. Kulić and A. I. Buzdin, *Superconductivity*, edited by K. H. Bennemann and J. B. Ketterson (Springer, Berlin, 2008) Chap. 4. Coexistence of Singlet Superconductivity and Magnetic Order in Bulk Magnetic Superconductors and SF Heterostructures, p. 163.
[15] K.-H. Müller and V. N. Narozhnyi, Interaction of superconductivity and magnetism in borocarbide superconductors, Rep. Prog. Phys. **64**, 943 (2001).
[16] L. C. Gupta, Superconductivity and magnetism and their interplay in quaternary borocarbides RNi_2B_2C, Adv. Phys. **55**, 691 (2006).
[17] C. T. Wolowiec, B. D. White, and M. B. Maple, Conventional magnetic superconductors, Physica C **514**, 113 (2015).
[18] M. A. Ruderman and C. Kittel, Indirect exchange coupling of nuclear magnetic moments by conduction electrons, Phys. Rev. **96**, 99 (1954); T. Kasuya, A Theory of Metallic Ferro- and Antiferromagnetism on Zener's Model, Progr. Theor. Phys. **16**, 45 (1956); K. Yosida, Magnetic properties of Cu-Mn alloys, Phys. Rev. **106**, 893 (1957).
[19] U. Krey, Micromagnetic theory of ferromagnetic superconductors, Int. J. Magn. **3**, 65 (1972); On the vortex lattice in magnetic superconductors, **4**, 153 (1973).
[20] M. Tachiki, H. Matsumoto, and H. Umezawa, Mixed state in magnetic superconductors, Phys. Rev. B **20**, 1915 (1979).
[21] P. W. Anderson and H. Suhl, Spin alignment in the superconducting state, Phys. Rev. **116**, 898 (1959).
[22] L. N. Bulaevskii, A. I. Rusinov, and M. Kulić, Helical ordering of spins in a superconductor, J. Low Temp. Phys. **39**, 255 (1980).
[23] H. Matsumoto, H. Umezawa, and M. Tachiki, A new phase in the magnetic superconductors, Solid State Commun. **31**, 157 (1979).
[24] H. S. Greenside, E. I. Blount, and C. M. Varma, Possible coexisting superconducting and magnetic states, Phys. Rev. Lett. **46**, 49 (1981).
[25] M. B. Maple and Ø. Fischer, eds., *Superconductivity in Ternary Compounds II, Superconductivity and Magnetism* (Springer, 1982).
[26] W. A. Fertig, D. C. Johnston, L. E. DeLong, R. W. McCallum, M. B. Maple, and B. T. Matthias, Destruction of superconductivity at the onset of long-range magnetic order in the compound $ErRh_4B_4$, Phys. Rev. Lett. **38**, 987 (1977).
[27] M. Ishikawa and Ø. Fischer, Destruction of superconductivity by magnetic ordering in $Ho_{1.2}Mo_6S_8$, Solid State Commun. **23**, 37 (1977).
[28] J. P. Remeika, G. P. Espinosa, A. S. Cooper, H. Barz, J. M. Rowell, D. B. McWhan, J. M. Vandenberg, D. E. Moncton, Z. Fisk, L. D. Woolf, H. C. Hamaker, M. B. Maple, G. Shirane, and W. Thomlinson, A new family of ternary intermetallic superconducting/magnetic stannides, Solid State Commun. **34**, 923 (1980).
[29] K.-H. Müller, M. Schneider, G. Fuchs, and S.-L. Drechsler, Chapter 239 - Rare-Earth Nickel Borocarbides, in *Handbook on the Physics and Chemistry of Rare Earths*, Vol. 38, edited by K. A. Gschneidner, J.-C. G. Bünzli, and V. K. Pecharsky (Elsevier, 2008) pp. 175–336.
[30] C. Mazumdar and R. Nagarajan, Quaternary borocarbides: Relatively high T_c intermetallic superconductors and magnetic superconductors, Physica C **514**, 173 (2015).
[31] D. Aoki and J. Flouquet, Ferromagnetism and superconductivity in uranium compounds, J. Phys. Soc. Jpn. **81**, 011003 (2012); D. Aoki, K. Ishida, and J. Flouquet, Review of u-based ferromagnetic superconductors: Comparison between UGe_2, URhGe, and UCoGe, **88**, 022001 (2019).
[32] A. D. Huxley, Ferromagnetic superconductors, Physica C **514**, 368 (2015).
[33] Y. Xiao, Y. Su, W. Schmidt, K. Schmalzl, C. M. N. Kumar, S. Price, T. Chatterji, R. Mittal, L. J. Chang, S. Nandi, N. Kumar, S. K. Dhar, A. Thamizhavel, and T. Brueckel, Field-induced spin reorientation and giant spin-lattice coupling in $EuFe_2As_2$, Phys. Rev. B **81**, 220406(R) (2010).
[34] C. F. Miclea, M. Nicklas, H. S. Jeevan, D. Kasinathan,

Z. Hossain, H. Rosner, P. Gegenwart, C. Geibel, and F. Steglich, Evidence for a reentrant superconducting state in $EuFe_2As_2$ under pressure, Phys. Rev. B **79**, 212509 (2009); T. Terashima, M. Kimata, H. Satsukawa, A. Harada, K. Hazama, S. Uji, H. S. Suzuki, T. Matsumoto, and K. Murata, $EuFe_2As_2$ under high pressure: An antiferromagnetic bulk superconductor, J. Phys. Soc. Jpn. **78**, 083701 (2009).

[35] Y. Qi, Z. Gao, L. Wang, D. Wang, X. Zhang, and Y. Ma, Superconductivity at 34.7K in the iron arsenide $Eu_{0.7}Na_{0.3}Fe_2As_2$, New J. Phys. **10**, 123003 (2008).

[36] U. B. Paramanik, P. L. Paulose, S. Ramakrishnan, A. K. Nigam, C. Geibel, and Z. Hossain, Magnetic and superconducting properties of Ir-doped $EuFe_2As_2$, Supercond. Sci. Technol. **27**, 075012 (2014).

[37] W.-H. Jiao, Q. Tao, J.-K. Bao, Y.-L. Sun, C.-M. Feng, Z.-A. Xu, I. Nowik, I. Felner, and G.-H. Cao, Anisotropic superconductivity in $Eu(Fe_{0.75}Ru_{0.25})_2As_2$ ferromagnetic superconductor, EPL (Europhysics Letters) **95**, 67007 (2011).

[38] S. Jiang, H. Xing, G. Xuan, Z. Ren, C. Wang, Z.-a. Xu, and G. Cao, Superconductivity and local-moment magnetism in $Eu(Fe_{0.89}Co_{0.11})_2As_2$, Phys. Rev. B **80**, 184514 (2009); Y. He, T. Wu, G. Wu, Q. J. Zheng, Y. Z. Liu, H. Chen, J. J. Ying, R. H. Liu, X. F. Wang, Y. L. Xie, Y. J. Yan, J. K. Dong, S. Y. Li, and X. H. Chen, Evidence for competing magnetic and superconducting phases in superconducting $Eu_{1-x}Sr_xFe_{2-y}Co_yAs_2$ single crystals, J. Physics: Condens. Matter **22**, 235701 (2010); Z. Guguchia, S. Bosma, S. Weyeneth, A. Shengelaya, R. Puzniak, Z. Bukowski, J. Karpinski, and H. Keller, Anisotropic magnetic order of the eu sublattice in single crystals of $EuFe_{2-x}Co_xAs_2$ ($x = 0, 0.2$) studied by means of magnetization and magnetic torque, Phys. Rev. B **84**, 144506 (2011); W. T. Jin, S. Nandi, Y. Xiao, Y. Su, O. Zaharko, Z. Guguchia, Z. Bukowski, S. Price, W. H. Jiao, G. H. Cao, and T. Brückel, Magnetic structure of superconducting $Eu(Fe_{0.82}Co_{0.18})_2As_2$ as revealed by single-crystal neutron diffraction, **88**, 214516 (2013).

[39] Y. Tokiwa, S.-H. Hübner, O. Beck, H. S. Jeevan, and P. Gegenwart, Unique phase diagram with narrow superconducting dome in $EuFe_2(As_{1-x}P_x)_2$ due to Eu^{2+} local magnetic moments, Phys. Rev. B **86**, 220505(R) (2012).

[40] S. Zapf, H. S. Jeevan, T. Ivek, F. Pfister, F. Klingert, S. Jiang, D. Wu, P. Gegenwart, R. K. Kremer, and M. Dressel, $EuFe_2(As_{1-x}P_x)_2$: Reentrant spin glass and superconductivity, Phys. Rev. Lett. **110**, 237002 (2013).

[41] S. Nandi, W. T. Jin, Y. Xiao, Y. Su, S. Price, D. K. Shukla, J. Strempfer, H. S. Jeevan, P. Gegenwart, and T. Brückel, Coexistence of superconductivity and ferromagnetism in P-doped $EuFe_2As_2$, Phys. Rev. B **89**, 014512 (2014).

[42] I. S. Veshchunov, L. Y. Vinnikov, V. S. Stolyarov, N. Zhou, Z. X. Shi, X. F. Xu, S. Y. Grebenchuk, D. S. Baranov, I. A. Golovchanskiy, S. Pyon, Y. Sun, W. Jiao, G. Cao, T. Tamegai, and A. A. Golubov, Visualization of the magnetic flux structure in phosphorus-doped $EuFe_2As_2$ single crystals, JETP Letters **105**, 98 (2017).

[43] V. S. Stolyarov, I. S. Veshchunov, S. Y. Grebenchuk, D. S. Baranov, I. A. Golovchanskiy, A. G. Shishkin, N. Zhou, Z. Shi, X. Xu, S. Pyon, Y. Sun, W. Jiao, G.-H. Cao, L. Y. Vinnikov, A. A. Golubov, T. Tamegai, A. I. Buzdin, and D. Roditchev, Domain Meissner state and spontaneous vortex-antivortex generation in the ferromagnetic superconductor $EuFe_2(As_{0.79}P_{0.21})_2$, Sci. Adv. **4**, eaat1061 (2018).

[44] Z. Devizorova, S. Mironov, and A. Buzdin, Theory of magnetic domain phases in ferromagnetic superconductors, Phys. Rev. Lett. **122**, 117002 (2019).

[45] J.-K. Bao, K. Willa, M. P. Smylie, H. Chen, U. Welp, D. Y. Chung, and M. G. Kanatzidis, Single crystal growth and study of the ferromagnetic superconductor $RbEuFe_4As_4$, Crystal Growth & Design **18**, 3517 (2018).

[46] M. P. Smylie, K. Willa, J.-K. Bao, K. Ryan, Z. Islam, H. Claus, Y. Simsek, Z. Diao, A. Rydh, A. E. Koshelev, W.-K. Kwok, D. Y. Chung, M. G. Kanatzidis, and U. Welp, Anisotropic superconductivity and magnetism in single-crystal $RbEuFe_4As_4$, Phys. Rev. B **98**, 104503 (2018).

[47] V. S. Stolyarov, A. Casano, M. A. Belyanchikov, A. S. Astrakhantseva, S. Y. Grebenchuk, D. S. Baranov, I. A. Golovchanskiy, I. Voloshenko, E. S. Zhukova, B. P. Gorshunov, A. V. Muratov, V. V. Dremov, L. Y. Vinnikov, D. Roditchev, Y. Liu, G.-H. Cao, M. Dressel, and E. Uykur, Unique interplay between superconducting and ferromagnetic orders in $EuRbFe_4As_4$, Phys. Rev. B **98**, 140506(R) (2018).

[48] K. Willa, R. Willa, J.-K. Bao, A. E. Koshelev, D. Y. Chung, M. G. Kanatzidis, W.-K. Kwok, and U. Welp, Strongly fluctuating moments in the high-temperature magnetic superconductor $RbEuFe_4As_4$, Phys. Rev. B **99**, 180502(R) (2019).

[49] D. E. Jackson, D. VanGennep, W. Bi, D. Zhang, P. Materne, Y. Liu, G.-H. Cao, S. T. Weir, Y. K. Vohra, and J. J. Hamlin, Superconducting and magnetic phase diagram of $RbEuFe_4As_4$ and $CsEuFe_4As_4$ at high pressure, Phys. Rev. B **98**, 014518 (2018).

[50] L. Xiang, S. L. Bud'ko, J.-K. Bao, D. Y. Chung, M. G. Kanatzidis, and P. C. Canfield, Pressure-temperature phase diagram of the $EuRbFe_4As_4$ superconductor, Phys. Rev. B **99**, 144509 (2019).

[51] K. Iida, Y. Nagai, S. Ishida, M. Ishikado, N. Murai, A. D. Christianson, H. Yoshida, Y. Inamura, H. Nakamura, A. Nakao, K. Munakata, D. Kagerbauer, M. Eisterer, K. Kawashima, Y. Yoshida, H. Eisaki, and A. Iyo, Coexisting spin resonance and long-range magnetic order of Eu in $EuRbFe_4As_4$, Phys. Rev. B **100**, 014506 (2019).

[52] Z. Islam *et al.*, unpublished.

[53] H. Benson and D. L. Mills, Spin waves in thin films; dipolar effects, Phys. Rev. **178**, 839 (1969); S. V. Maleev, Dipole forces in two-dimensional and layered ferromagnets, [Zh. Eksp. Teor. Fiz. **70**, 2374 (1976)] JETP **43**, 1240 (1976).

[54] A. Akbari, P. Thalmeier, and I. Eremin, Evolution of the multiband Ruderman–Kittel–Kasuya–Yosida interaction: application to iron pnictides and chalcogenides, New J. Phys. **15**, 033034 (2013).

[55] Z. Devizorova and A. Buzdin, Superconductivity-driven helical magnetic structure in $EuRbFe_4As_4$ ferromagnetic superconductor, Phys. Rev. B **100**, 104523 (2019).

[56] L. M. Roth, H. J. Zeiger, and T. A. Kaplan, Generalization of the Ruderman-Kittel-Kasuya-Yosida interaction for nonspherical Fermi surfaces, Phys. Rev. **149**, 519 (1966).

[57] D. N. Aristov, Indirect RKKY interaction in any dimensionality, Phys. Rev. B **55**, 8064 (1997).

[58] B. I. Kochelaev, L. R. Tagirov, and M. G. Khusainov, Spatial dispersion of spin susceptibility of conduction

electrons in a superconductor, [Zh. Eksp. Teor. Fiz. **76**, 578 (1979)] JETP **49**, 291 (1979).

[59] F. Lochner, F. Ahn, T. Hickel, and I. Eremin, Electronic properties, low-energy hamiltonian, and superconducting instabilities in $CaKFe_4As_4$, Phys. Rev. B **96**, 094521 (2017).

[60] C. Xu, Q. Chen, and C. Cao, Unique crystal field splitting and multiband RKKY interactions in Ni-doped $EuRbFe_4As_4$, Commun. Phys. **2**, 16 (2019).

[61] P. Bak, Commensurate phases, incommensurate phases and the devil's staircase, Rep. Prog. Phys. **45**, 587 (1982).

[62] V. L. Pokrovsky, A. L. Talapov, and P. Bak, *Solitons*, edited by S. E. Trullinger, V. E. Zakharov, and V. L. Pokrovsky, Modern problems in condensed matter sciences, v. 17 (North-Holland, Amsterdam, 1986) p. 71.

[63] T. Nagamiya, Helical spin ordering–1 Theory of helical spin configurations, in *Solid State Physics*, Vol. 20, edited by F. Seitz, D. Turnbull, and H. Ehrenreich (Academic Press, 1968) pp. 305–411.

[64] D. C. Johnston, Unified molecular field theory for collinear and noncollinear heisenberg antiferromagnets, Phys. Rev. B **91**, 064427 (2015).